J Mater Sci (2017) 52:13192–13202

Energy materials

Ionic liquid-derived Co_3O_4/carbon nano-onions composite and its enhanced performance as anode for lithium-ion batteries

Yanshuang Meng[1,3], Gongrui Wang[1], Mingjun Xiao[1], Chaoyu Duan[1], Chen Wang[1], Fuliang Zhu[1,3,*], and Yue Zhang[2,*]

[1] School of Materials Science and Engineering, Lanzhou University of Technology, Lanzhou 730050, China
[2] Department of Mechanical and Industrial Engineering, Texas A&M University-Kingsville, Kingsville, TX 78363, USA
[3] State Key Laboratory of Advanced Processing and Recycling of Non-ferrous Metals, Lanzhou 730050, China

Received: 3 June 2017
Accepted: 19 July 2017
Published online: 26 July 2017

© Springer Science+Business Media, LLC 2017

ABSTRACT

In this work, a novel composite of Co_3O_4 nanoparticle and carbon nano-onions (CNOs) is synthesized by using ionic liquid as carbon and nitrogen source through a facile carbothermic reduction followed by low-temperature oxidation method. The SEM and HRTEM images reveal that the Co_3O_4 particles are homogenously embedded in the CNOs. Due to the unique nano-structure, the electrolyte contacts well with the active materials, leading to a better transfer of lithium ions. Moreover, the unique nano-structure not only buffers the volume changes but also facilitates the shuttling of electrons during the cycling process. As a result, the electrode made up of Co_3O_4/CNOs composite delivers favorable cycling performance (676 mAh g^{-1} after 200 cycles) and rate capability (557 mAh g^{-1} at the current of 1 C), showing a promising prospect for lithium-ion batteries as anode materials.

Introduction

Lithium-ion batteries (LIBs) have been identified as one of the most important energy storage devices as their applications have been successfully expanded from small-scale portable electronics to large-scale electronic vehicles [1]. Previous researches indicated that the electrode material, especially the anode material, plays a critical role in determining the performance of LIBs [2, 3]. Graphite is a commonly used anode material in commercial LIBs; however, a theoretical capacity of only 372 mAh g^{-1} significantly limited its LIB performance [4]. Conversion reaction-based transition metal oxides, including SnO_2 [5], CuO [6], Fe_3O_4 [7], and Co_3O_4 [8], are attractive candidates for LIB anodes. Among these metal oxides, Co_3O_4 has received extensive attention of researches, because of its many beneficial properties such as excellent reversible redox behavior, good corrosion stability, its simple preparation method, and promising ratio of surface atoms and diverse morphologies [9–11]. More importantly, it shows

Address correspondence to E-mail: chzfl@126.com; yue.zhang@tamuk.edu

DOI 10.1007/s10853-017-1414-x

huge development potential due to its high theoretical capacity (890 mAh g^{-1}) when compared with conventional graphite electrodes [12, 13]. However, the wide application of Co_3O_4 electrodes is hindered by its low inherent conductivity and large volume variation during lithiation/delithiation, which can lead to pulverization, electrochemical sintering, and eventually a capacity fading [14, 15].

To overcome these shortcomings, numerous methods have been investigated, including nano-crystallization [16], combination with other oxide materials [17, 18], and incorporation with carbon materials [19–21]. Among these methods, incorporating carbon materials with Co_3O_4 becomes the focus of researches recently as this method exhibits the potential to achieve the best electrochemical and dynamic performance. The integrated carbon materials, such as reduced graphene oxide [22, 23], carbon nanotubes [20], carbon nanofiber [24, 25], hollow carbon spheres [26], porous carbon [27], and onion-like carbon [28–30], can not only buffer the volume changes but also facilitate the shuttling of electrons, leading to an enhanced electrical conductivity during cycling process.

Ionic liquids (ILs) have been studied to a lesser extend as carbon source but are gaining increased interests recently for applications in LIBs due to its negligible vapor pressure and designable structure [31–35]. The negligible vapor of ILs moderates the evaporation of ILs during the carbonizations process, which makes the processing and shaping process simple to implement. The designable structure allows a controllable ratio of cation and anion components in ILs, which can tune the doping contents of heteroatoms in the carbon materials.

In this work, we have produced Co_3O_4/CNOs composites by using 1-butyl-3-methylimidazolium dicyanamide (BMIm)$N(CN)_2$ as carbon and nitrogen source. The composite was first characterized by a variety of techniques including powder X-ray diffraction (XRD), Raman spectroscopy, X-ray photoelectron spectroscopy (XPS), and electron microscopy to determine the quality of the electrode materials. The material was assembled into coin-type half cells to measure the electrochemical properties. Because of the onion-like structure of the carbon component, the interfaces of carbon and Co_3O_4 particles are well developed, leading to a symmetrical acceleration of electron shuttling and subsequently improved electrochemical performance.

Experimental section

Material synthesis

The Co_3O_4/CNOs composite is synthesized through direct pyrolysis of ionic liquid precursor and cobalt(II) acetate tetrahydrate ($C_4H_6CoO_4{\cdot}4H_2O$, Aladdin AR 99.5%), followed by low-temperature oxidation. In a specific preparation method, 0.517 g $C_4H_6CoO_4{\cdot}4H_2O$ is dissolved in 2 ml ultrapure water, followed by adding 1 g of (BMIm)$N(CN)_2$ (purchased from Lanzhou Institute of Chemical Physics, Chinese Academy of Sciences). After that, the mixture is ground in the agate mortar for 30 min at room temperature (Fig. 1a). The material is transferred into a ceramic crucible and dried at 100 °C for 15 h in the air blowing thermostatic oven (Fig. 1b). The as-obtained material is annealed at 350 °C for 30 min and then at 700 °C for 1 h in the tube furnace with the protection of an argon atmosphere. The material is oxidized by heating treatment at 250 °C for 0.5 h for Co_3O_4/CNOs composite and 10 h for bare Co_3O_4 in the ambient atmosphere, respectively (Fig. 1c).

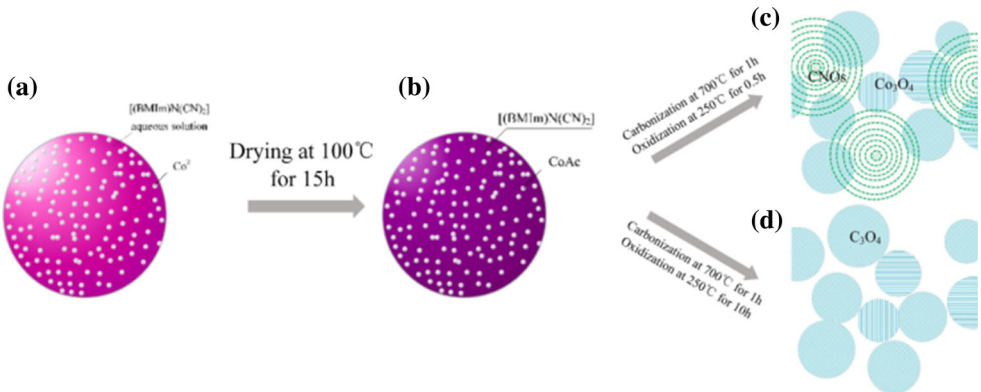

Figure 1 Schematic of the synthesis process for Co_3O_4/CNOs composites and bare Co_3O_4.

Material characterization

The phase composition of the as-synthesized material is characterized by powder XRD (D/max-2400, Cu Kα). Further information of the materials is investigated using Raman on a LabRAM HR800 equipment and the XPS on a Kratos XSAM 800 spectrometer. The morphology and microstructure are determined by scanning electron microscope (SEM) on a Quanta450FEG equipment and transmission electron microscopy (TEM) and high-resolution TEM (HRTEM) on a JEM-1200EX equipment. The carbon and nitrogen element contents are characterized by Elementar Analysensysteme GmbH VarioEL cube. The Brunauer–Emmett–Teller nitrogen adsorption–desorption measurement of the as-synthesized material is taken on a Micromeritics ASAP 2020 equipment.

Electrochemical measurement

The electrochemical performance of the as-obtained material is tested by using CR2032-type coin cells fabricated in an argon-filled glove box. The coating slurry is manufactured by active materials, acetylene black, and polyvinylidene fluoride (PVDF) with a mass ratio of 7:2:1. The working electrode is fabricated by painting the slurry onto copper foils and then dried at 100 °C for 10 h in a vacuum oven

The cyclic voltammetry (CV) measurement is employed to characterize the reaction potential and reaction type on a CHI660E electrochemical workstation at a scan rate of 0.1 mV s^{-1} in a voltage range of 0–3 V (vs. Li/Li^+). The capacity and cycling performances are measured by galvanostatic discharge/charge measurement with a specific current of 89 mA g^{-1} in the voltage range of 0.01–3 V (vs. Li/Li^+) on a battery test system (LAND CT2001A, China). The rate properties are carried out at various specific current densities 0.1, 0.2, 0.3, 0.5, 1, and 0.1 C.

Results and discussion

The XRD patterns of the Co_3O_4/CNOs composite and bare Co_3O_4 are shown in Fig. 2a. Both samples exhibit peaks at 18.8°, 31.1°, 36.9°, 38.2°, 44.8°, 55.4°, 59.4°, 65.2°, and 77.5°, which corresponds to the face-centered cubic phase of spinel-structured Co_3O_4 (JCPDS No. 42-1467) [36, 37]. In the spectrum of Co_3O_4/CNOs composite, the compressed diffraction peak (as shown in Fig. 2b) at 23.8° is designated as the (002) reflection of graphite (JCPDS No. 41-1487) [38, 39]. When compared with the Co_3O_4/CNOs composite, the bare Co_3O_4 sample has shaper peaks, indicating that extended heating can facilitate to achieve a high phase purity and crystal degree of Co_3O_4.

The Raman spectrum of Co_3O_4/CNOs composite further confirms the formation of carbon (Fig. 2c). The broad Raman scattering peaks located at 1358 and 1587 cm^{-1} can be assigned to the D and G band, arousing from the sp^3 and sp^2 hybridization vibrations of carbon materials, respectively [13]. No D or G band is observed in the spectrum of bare Co_3O_4, indicating that the carbon material is fully removed after heating in air for 10 h. The distinct peaks at 196, 481, 524, 619, and 686 cm^{-1} are attributed to the B_{1g}, E_g, F^1_{2g}, F^2_{2g}, and A_{1g} vibration mode of Co_3O_4, respectively [12, 13, 40], certifying the existence of Co_3O_4 in both samples.

The XPS analysis, shown in Fig. 3, shows the near-surface chemical information of the Co_3O_4/CNOs composite. The convolution Co 2p spectrum is exhibited in Fig. 3a. The peaks centered at 780.6 and 795.9 eV are ascribed to Co $2p_{3/2}$ and Co $2p_{1/2}$ spin-orbital peaks of Co_3O_4, respectively [41]. This indicates that the Co species in the composites exist in the form of Co_3O_4, which is in agreement with the XRD and Raman results. The strong shake-up peaks located at 795.9 and 804.2 eV further confirm the presence of Co_3O_4 [42]. The spectrum of O 1s can be split into two peaks at 530.1 and 531.3 eV, corresponding to the Co–O and C–O bonds, respectively (Fig. 3b) [43]. As displayed in Fig. 3c, the high-resolution XPS spectrum of C 1s is deconvoluted into three peaks at 284.7, 285.6, and 286.5 eV, respectively. The peak centered at 284.7 eV is assigned to the sp^2 hybridized carbon, corresponding to C–C bonds or C=C bonds [44]. The peak located at 285.6 eV is ascribed to C=N bonds or C–O bonds [15, 45], which may arise from the nitrogenous carbon precursors and C–O–Co bonds that combine carbon materials with Co_3O_4 [46]. The peak at 286.5 eV is designated to C–N or C=O bonds [45, 47, 48]. Figure 3d exhibits the N 1s XPS spectrum, which indicates the presence of pyridinic N (398.7 eV), pyrrolic N (399.6 eV), and graphitic N (400.1 eV) [42]. Previous researches have reported that N-doped carbon can enhance conductivity, electrochemical activity, and stability [15, 49]. Particularly, the pyridinic and graphitic nitrogen atoms can facilitate the absorption of lithium ions, which

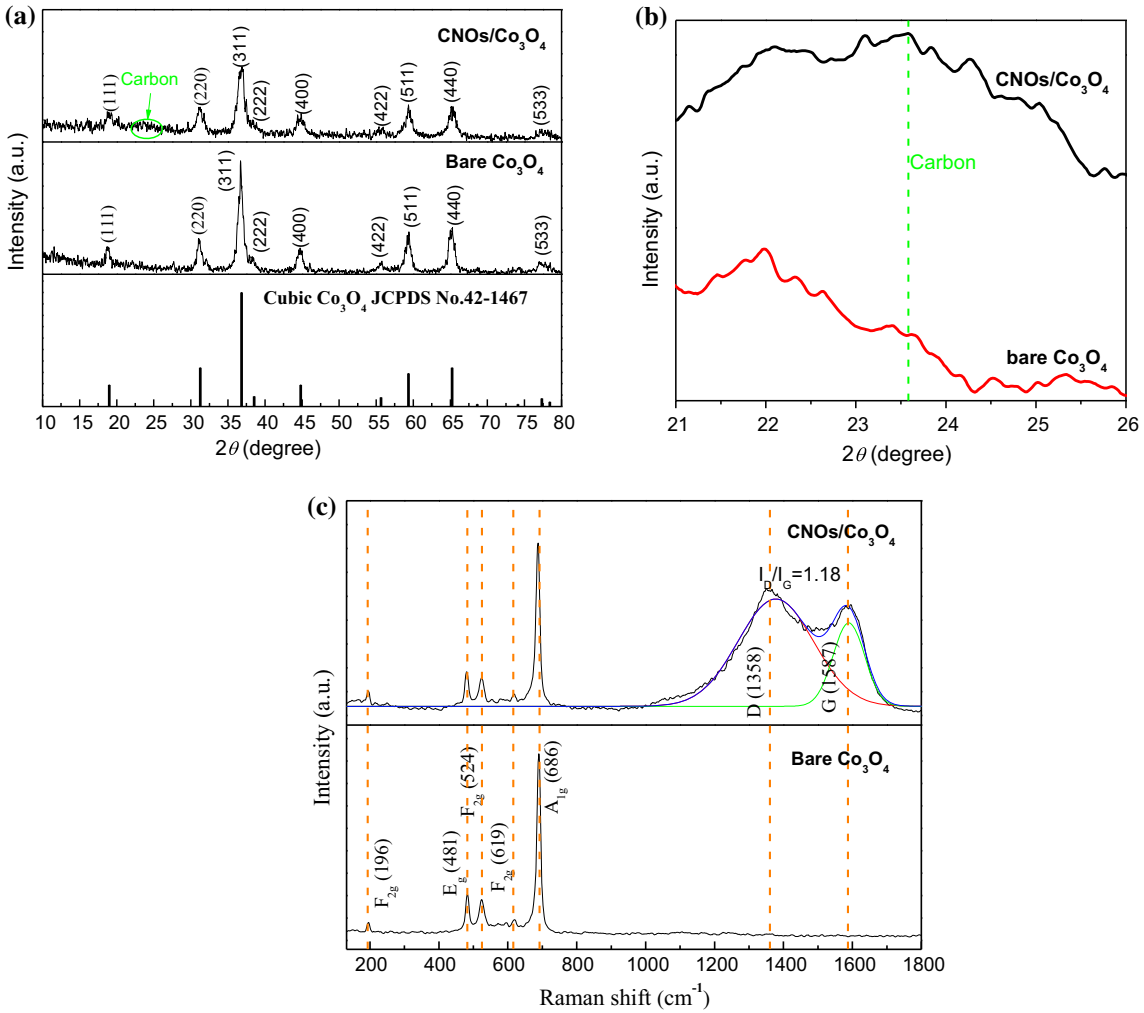

Figure 2 XRD patterns (**a**, **b**) and Raman spectra (**c**) of Co_3O_4/CNOs composite and bare Co_3O_4.

contributes to the capacity of the as-synthesized Co_3O_4/CNOs composite [50].

The electron microscopy is applied to observe the morphology of the Co_3O_4/CNOs composites (Fig. 4). As displayed in Fig. 4a, the SEM image reveals a nano-structure with Co_3O_4 embedding in CNOs, which is accompanied with trivial agglomeration of the particles with uniform distributed grain size. Due to this unique nano-structure, the electrolyte contacts well with the active materials, leading to a better transfer of lithium ions. Figure 4b and its inset present the TEM image and selected area electron diffraction (SEAD) patterns of as-prepared Co_3O_4/CNOs composites. The TEM image provides further information of the composites, showing that the particles observed in SEM image are constituted of smaller particles. The SEAD patterns exhibit the typical diffraction rings of Co_3O_4 which is denoted by blue line. The diffraction ring of carbon, denoted by green line, is faint and broadened, which indicates the content of CNOs is low. A close view of region 1 and region 2 in Fig. 4b is shown in Fig. 4c, d. From the test of Fourier transform algorithm, it is found that the particles marked with blue dashed circle in Fig. 4c, d are Co_3O_4 particles. The particles in Fig. 4c display an interplanar spacing of 0.244 nm, corresponding to the (311) plane of spinel-structured Co_3O_4 (JCPDS No. 42-1467). The materials in the green dashed circle are carbon that exists in the form of CNOs. The formation of CNOs is because of the catalysis effects of Co_3O_4 particles and metallic cobalt that is formed in the pilot process [51, 52]. Due to the surface energy minimization effect, the CNOs are in the form of sphere. The Co_3O_4 particles are

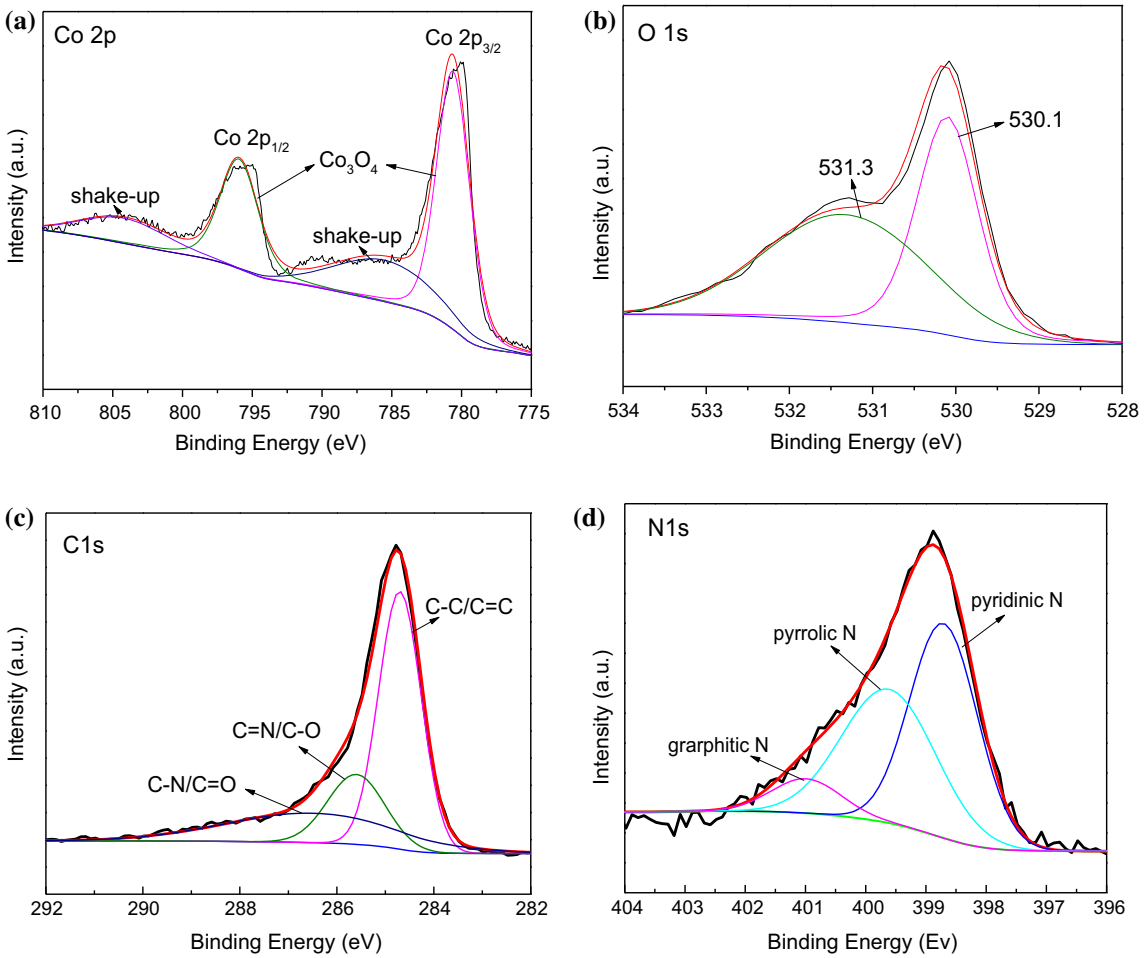

Figure 3 High-resolution XPS spectra of Co_3O_4/CNOs composite: **a** Co2p, **b** C1s, **c** N1s, and **d** O1s.

embedded in the CNOs and partially expose to the external environment due to the oxidization process above 300 °C which evaporates carbon materials.

As shown in Fig. 5, N^2 adsorption/desorption experiments are performed to examine the pore size distribution and surface areas of the Co_3O_4/CNOs composite. The isotherms of Co_3O_4/CNOs composite are typical type curves according to IUPAC classification. The pore size distribution shows that the Co_3O_4/CNOs composite possessed a mesoporous structure with an average pore size of 3.2 nm. The BET surface area of Co_3O_4/CNOs composite is confirmed to be 79.79 $m^2\ g^{-1}$ which is in line with the observation in SEM image.

To investigate the electrochemical performance of the Co_3O_4/CNOs composite, Co_3O_4/CNOs-Li half battery is assembled, with the Co_3O_4/CNOs composite and metallic lithium as positive and negative electrodes, respectively. Figure 6a shows the first three CV curves of Co_3O_4/CNOs composite at a scan rate of 0.1 mV s^{-1}, over the voltage range of 0–3 V. A distinct and irreversible reductive peak at 0.89 V (A) is observed during the first cathodic scan. This peak is arisen by two reactions: (1) the electrochemical reduction reaction of Co_3O_4 and the formation of amorphous Li_2O ($Co_3O_4 + 8Li^+ + 8e^- \leftrightarrow 4Li_2O + 3Co^0$) and (2) the reductive decomposition reaction of $LiPF_6$ and organic solvent (EC and DEC) in which the solid electrolyte interphase (SEI) film is formed on the surface of the Co_3O_4/CNOs. The cathodic peak around below 0.47 V (C) stems from the intercalation of Li^+ ions into CNOs of the Co_3O_4/CNOs composite [53], indicating the electrochemical activity of CNOs. In the first anodic scan, the unambiguous peaks at 1.32 V (A′) and 2.07 V (A″) are distinguished and designated to the conversion reaction of $Co^0 + xLi_2O \leftrightarrow CoO_x + 2xLi^+ + 2xe^-$ (CoO_x refers to CoO or Co_3O_4), certifying that the

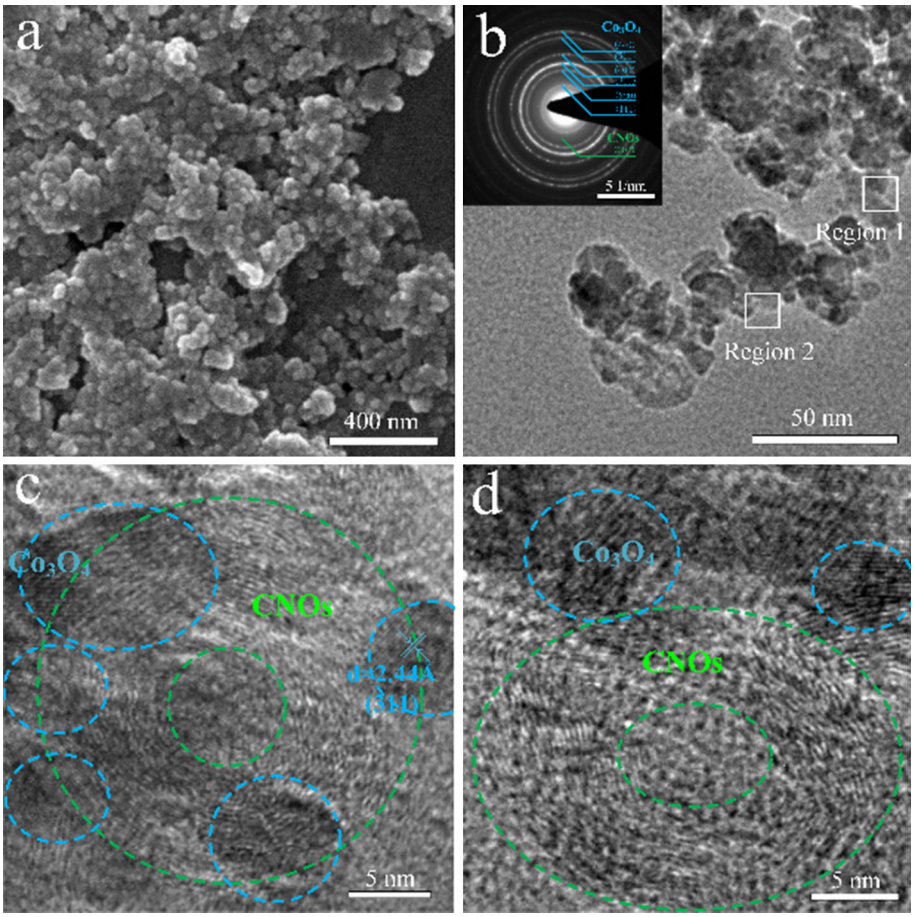

Figure 4 SEM (**a**), TEM (**b**), HRTEM images (**c**, **d**), and SAED patterns (*inset* of **b**) of Co_3O_4/CNOs composite.

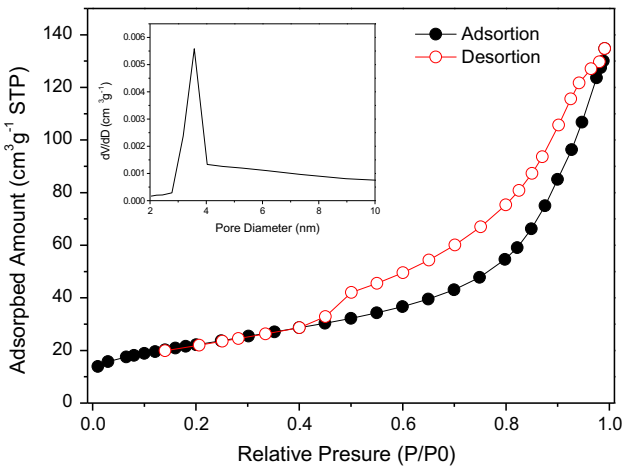

Figure 5 Nitrogen adsorption–desorption isotherms of the Co_3O_4/CNOs composite and the pore size distribution curve (*inset* picture).

oxidization of Co^0 to Co_3O_4 is a multistep reaction [54, 55]. The reduction peak at 0.89 V (A) in the first cathodic scan shows a shift and is split into two lower-intensity and broad peaks at 1.24 and 0.98 V, which are ascribed to the reduction reaction of Co_3O_4 and CoO [54, 56], respectively. The primary peaks of the third cycle are almost overlapped with the peaks of the second cycle, indicating a great reversibility and integrity of the electrode [57].

Figure 6b displays the discharge/charge profiles of the Co_3O_4/CNOs composite at a specific current density of 89 mA g^{-1}. There is a long voltage plateau at 1.01 V in the initial discharge process, which is attributed to the formation of SEI layers on active materials and the electrochemical reduction reaction of Co_3O_4 [58]. The voltage declines slowly to the cut voltage of 0.01 V after the long voltage plateau and eventually results in a discharge capacity of 1468 mAh g^{-1}. After that, the charge process displays two identifiable and gradient voltage plateau at 1.32 and 2.06 V, which are ascribed to the oxidation reaction of metallic cobalt particles and the decomposition of Li_2O [54, 55, 59]. The following curves are almost overlapped, showing a favorable reversibility of the Co_3O_4/CNOs composite.

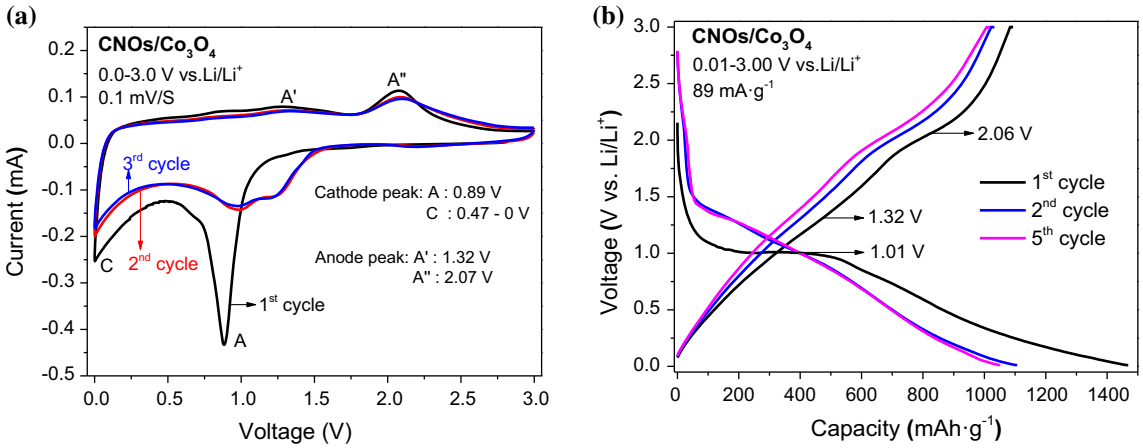

Figure 6 CV measurements (**a**) and the discharge/charge curves (**b**) of Co_3O_4/CNOs composite.

Figure 7 Galvanostatic charge–discharge profiles of Co_3O_4/CNOs composite and bare Co_3O_4 at 89 mA g^{-1}.

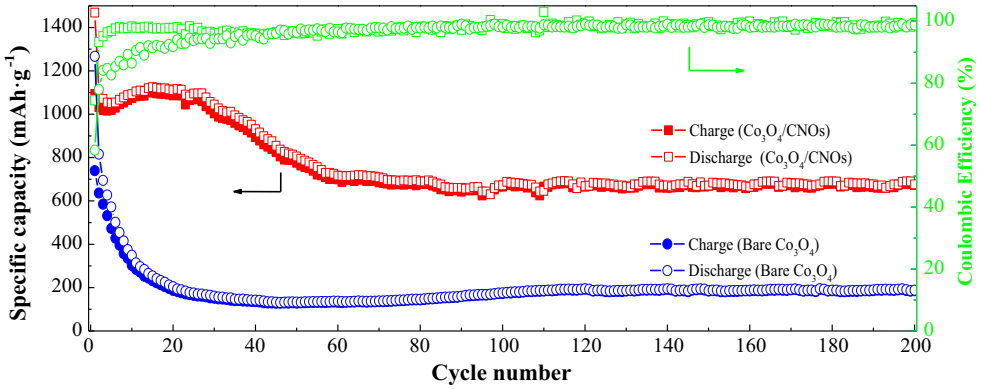

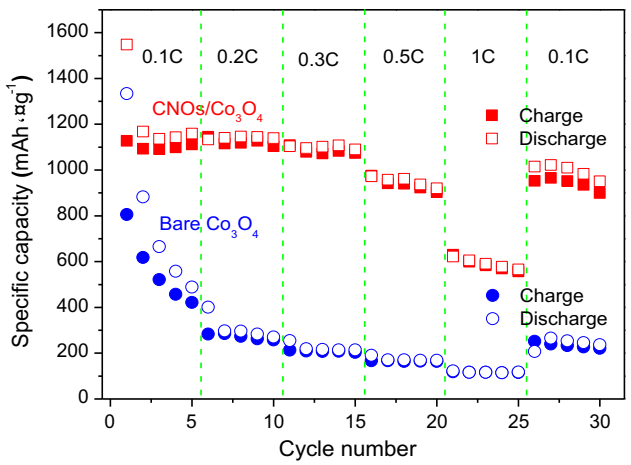

Figure 8 Rate performance of Co_3O_4/CNOs composite and bare Co_3O_4 at various current densities.

As exhibited in Fig. 7, the cycling performance of the Co_3O_4/CNOs composite and bare Co_3O_4 as anode materials is measured at a current density of 89 mAh g^{-1} over 0.1–3.00 V. The electrode of bare Co_3O_4 shows a reversible capacity of 172 mAh g^{-1}. For the electrode of Co_3O_4/CNOs composite, the first discharge and charge capacities are 1468 and 1093 mAh g^{-1}, respectively, with an initial coulombic efficiency of 74.47%. The initial discharge and charge capacities exceed the theoretical capacity of Co_3O_4/CNOs composite, which is estimated as follows:

$$\begin{aligned} C_{\text{theoretical}} &= C_{\text{graphite}} \times \text{mass ratio of carbon materials} \\ &\quad + C_{Co_3O_4} \times \text{mass ratio of } Co_3O_4 \\ &= 372\,\text{mAh}\,g^{-1} \times 6.24\% + 890\,\text{mAh}\,g^{-1} \\ &\quad \times 93.76\% = 857.7\,\text{mAh}\,g^{-1} \end{aligned}$$

The content of CNOs in the composites is tested by elemental analysis. The extra capacities of Co_3O_4/CNOs composite may be ascribed to the auxiliary lithium-ion storage sites, such as defects, grain boundaries of Li_2O, and the formation of metallic cobalt in the discharge process [36, 52, 60, 61]. Furthermore, the reversible formation/dissolution conversion reaction, following electrochemical catalytic conversion mechanism which refers to the effective catalysis of metallic cobalt and Co_3O_4 of SEI layers

during cycling, contributes to the extra discharge/charge capacities [60, 62]. The pyridinic and graphitic nitrogen atoms of Co_3O_4/CNOs can contribute to the capacity by facilitating the absorption of lithium ions [50]. Moreover, the enlarged (002) interplanar distance can provide lithium-ion storage sites [63].

After the first cycle, the reversible discharge/charge capacities increase gradually to 1120 and 1100 mAh g^{-1} at 15th cycle, respectively. The increased capacities are due to the reversible formation of pseudocapacitive polymeric film and the incremental lithium-ion storage sites among amorphous CoO_x that are formed from the conversion of the crystal state during the cycling process [16, 64, 65]. The bare Co_3O_4 electrode displays a sharp decrease in capacity after the first cycle, while the capacities of the Co_3O_4/CNOs electrode are stable and do not show any capacity decrease before the 30th cycle, which may be due to the carbon materials which serve as the protection layers of the Co_3O_4 particles. After the 30th cycle, the capacities of the Co_3O_4/CNOs electrode gradually reduce and become steady after the 60th cycle. The capacities reduction may be due to the nano-structure exfoliation caused by the constant volume variations during the cycling process. Because of the special structure, the Co_3O_4/CNOs electrode still performs a discharge and charge capacities of 676 and 672 mAh g^{-1} with a coulombic efficiency of 99% after 200 cycles.

As shown in Fig. 8, the rate performance of Co_3O_4/CNOs composite and bare Co_3O_4 is measured at 0.1, 0.2, 0.3, 0.5, 1, and 0.1 C for five cycles at each current density. For the bare Co_3O_4, the reversible capacities are 421, 257, 203, 163, 116, and 221 mAh g^{-1} at the current of 0.1, 0.2, 0.3, 0.5, 1, and 0.1 C, respectively. The Co_3O_4/CNOs composite presents a reversible capacity of 1111, 1103, 1073, 903, 557, and 898 mAh g^{-1} at the current of 0.1, 0.2, 0.3, 0.5, 1, and 0.1 C, respectively. The rate performance of Co_3O_4/CNOs composite is favorable compared with bare Co_3O_4 and cycling performance of Co_3O_4/CNOs composite. When compared with the bare Co_3O_4, the Co_3O_4/CNOs composite exhibits better rate performance and cycling performance.

Conclusions

A novel Co_3O_4/CNOs composite with homogenous nano-structure is synthesized via a facile method at low temperature by using (BMIm)$N(CN)_2$ as carbon and nitrogen source. The Co_3O_4/CNOs composite is consisted of Co_3O_4 nano-crystal and carbon nano-onions. The unique nano-structure can not only buffer the volume changes but also facilitate the shuttling of electron, which can promote the conductivity of the materials during cycling process. The electrode made up of Co_3O_4/CNOs composite delivers favorable cycling performance and rate capability, showing a promising prospect for LIBs as anode materials.

Acknowledgements

The project was supported by the National Natural Science Foundation of China (Grant Nos. 51364024, 51404124), Natural Science Foundation of Gansu Province (Grant No. 1506RJZA100), and the Foundation for Innovation Groups of Basic Research in Gansu Province (No. 1606RJIA322).

Compliance with ethical standards

Conflicts of interest The authors certify that they have no affiliations with or involvement in any organization or entity with any financial interest (such as honoraria; educational grants; participation in speakers' bureaus; membership, employment, consultancies, stock ownership, or other equity interest; and expert testimony or patent-licensing arrangements), or non-financial interest (such as personal or professional relationships, affiliations, knowledge, or beliefs) in the subject matter or materials discussed in this manuscript.

References

[1] Cheng X-B, Zhang Q, Wang H-F, Tian G-L, Huang J-Q, Peng H-J, Zhao M-Q, Wei F (2015) Nitrogen-doped herringbone carbon nanofibers with large lattice spacings and abundant edges: catalytic growth and their applications in lithium ion batteries and oxygen reduction reactions. Catal Today 249:244–251

[2] Liu X, Wu Y, Yang Z, Pan F, Zhong X, Wang J, Gu L, Yu Y (2015) Nitrogen-doped 3D macroporous graphene frameworks as anode for high performance lithium-ion batteries. J Power Sources 293:799–805

[3] Li Y, Lv X, Lu J, Li J (2010) Preparation of SnO_2-nanocrystal/graphene-nanosheets composites and their lithium storage ability. J Phys Chem C 114(49):21770–21774

[4] Wu Y-P, Rahm E, Holze R (2003) Carbon anode materials for lithium ion batteries. J Power Sources 114(2):228–236

[5] Park MS, Wang GX, Kang YM, Wexler D, Dou SX, Liu HK (2007) Preparation and electrochemical properties of SnO_2 nanowires for application in lithium-ion batteries. Angew Chem 119(5):764–767

[6] Gao S, Yang S, Shu J, Zhang S, Li Z, Jiang K (2008) Green fabrication of hierarchical CuO hollow micro/nanostructures and enhanced performance as electrode materials for lithium-ion batteries. J Phys Chem C 112(49):19324–19328

[7] Cui Z-M, Jiang L-Y, Song W-G, Guo Y-G (2009) High-yield gas–liquid interfacial synthesis of highly dispersed Fe_3O_4 nanocrystals and their application in lithium-ion batteries. Chem Mater 21(6):1162–1166

[8] Li D, Yang D, Zhu X, Jing D, Xia Y, Ji Q, Cai R, Li H, Che Y (2014) Simple pyrolysis of cobalt alginate fibres into Co_3O_4/C nano/microstructures for a high-performance lithium ion battery anode. J Mater Chem A 2(44):18761–18766

[9] Gou J, Xie S, Liu Y, Liu C (2016) Flower-like nickel-cobalt hydroxides converted from phosphites for high rate performance hybrid supercapacitor electrode materials. Electrochim Acta 210:915–924

[10] Yan D, Zhang H, Chen L, Zhu G, Li S, Xu H, Yu A (2014) Biomorphic synthesis of mesoporous Co_3O_4 microtubules and their pseudocapacitive performance. ACS Appl Mater Interfaces 6(18):15632–15637

[11] Xiao Y, Liu S, Feng L, Zhang A, Zhao J, Fang S, Jia D (2012) 3D Hierarchical Co_3O_4 twin-spheres with an urchin-like structure: large-scale synthesis, multistep-splitting growth, and electrochemical pseudocapacitors. Adv Funct Mater 22(19):4052–4059

[12] Numan A, Shahid MM, Omar FS, Ramesh K, Ramesh S (2017) Facile fabrication of cobalt oxide nanograin-decorated reduced graphene oxide composite as ultrasensitive platform for dopamine detection. Sensors Actuators B Chem 238:1043–1051

[13] Sun GL, Ma LY, Ran JB, Shen XY, Tong H (2016) Incorporation of homogeneous Co_3O_4 into a nitrogen-doped carbon aerogel via a facile in situ synthesis method: implications for high performance asymmetric supercapacitors. J Mater Chem A 4(24):9542–9554

[14] Hsieh C-T, Lin J-S, Chen Y-F, Teng H (2012) Pulse microwave deposition of cobalt oxide nanoparticles on graphene nanosheets as anode materials for lithium ion batteries. J Phys Chem C 116(29):15251–15258

[15] Zhang MM, Li R, Chang XX, Xue C, Gou XL (2015) Hybrid of porous cobalt oxide nanospheres and nitrogen-doped graphene for applications in lithium-ion batteries and oxygen reduction reaction. J Power Sources 290:25–34

[16] Zhou XY, Shi JJ, Liu Y, Su QM, Zhang J, Du GH (2014) Microwave irradiation synthesis of Co_3O_4 quantum dots/-graphene composite as anode materials for Li-ion battery. Electrochim Acta 143:175–179

[17] Won JM, Cho JS, Kang YC (2016) Superior electrochemical properties of SiO_2-doped Co_3O_4 hollow nanospheres obtained through nanoscale Kirkendall diffusion for lithium-ion batteries. J Alloy Compd 680:366–372

[18] Zhang YP, Zhuo QQ, Lv XX, Ma YY, Zhong J, Sun XH (2015) NiO-Co_3O_4 nanoplate composite as efficient anode in Li-ion battery. Electrochim Acta 178:590–596

[19] Wu BB, Zhang SL, Yao F, Huo RJ, Zhang FZ, Xu SL (2016) Nitrogen-doped carbon and high-content alumina containing bi-active cobalt oxides for efficient storage of lithium. J Colloid Interf Sci 462:183–190

[20] Wenelska K, Neef C, Schlestein L, Klingeler R, Kalenczuk RJ, Mijowska E (2015) Carbon nanotubes decorated by mesoporous cobalt oxide as electrode material for lithium-ion batteries. Chem Phys Lett 635:185–189

[21] Wang G, Meng Y, Wang L, Xia J, Zhu F, Zhang Y (2017) Yolk-shell Co_3O_4–CoO/carbon composites for lithium-ion batteries with enhanced electrochemical properties. Int J Electrochem Sci 12:2618–2627

[22] Zhang DH, Zou WB (2013) Decorating reduced graphene oxide with Co_3O_4 hollow spheres and their application in supercapacitor materials. Curr Appl Phys 13(8):1796–1800

[23] Xu YN, Wang XF, An CH, Wang YJ, Jiao LF, Yuan HT (2014) Synthesis of cobalt oxide-reduced graphene nanocomposite and its enhanced electrochemical properties as negative material for alkaline secondary battery. J Power Sources 272:328–334

[24] Yao WL, Yang J, Wang JL, Tao LA (2008) Synthesis and electrochemical performance of carbon nanofiber-cobalt oxide composites. Electrochim Acta 53(24):7326–7330

[25] Yao WL, Wang JL, Yang J, Du GD (2008) Novel carbon nanofiber-cobalt oxide composites for lithium storage with large capacity and high reversibility. J Power Sources 176(1):369–372

[26] Zhan L, Wang YL, Qiao WM, Ling LC, Yang SB (2012) Hollow carbon spheres with encapsulation of Co_3O_4 nanoparticles as anode material for lithium ion batteries. Electrochim Acta 78:440–445

[27] Wu JF, Zuo L, Song YH, Chen YQ, Zhou RH, Chen SH, Wang L (2016) Preparation of biomass-derived hierarchically porous carbon/Co_3O_4 nanocomposites as anode materials for lithium-ion batteries. J Alloy Compd 656:745–752

[28] Abouelsayed A, Anis B, Hassaballa S, Khalil ASG, Rashed UM, Eid KA, Al-Ashkar E, El hotaby W (2017) Preparation, characterization, Raman, and terahertz spectroscopy study

on carbon nanotubes, graphene nano-sheets, and onion like carbon materials. Mater Chem Phys 189:127–135

[29] Zhu C, Xu F, Chen J, Min H, Dong H, Tong L, Qasim K, Li S, Sun L (2016) Nitrogen-doped carbon onions encapsulating metal alloys as efficient and stable catalysts for dye-sensitized solar cells. J Power Sources 303:159–167

[30] Asokan V, Nørgaard Madsen D, Kosinski P, Myrseth V (2015) Transformation of carbon black into carbon nano-beads and nanotubes: the effect of catalysts. New Carbon Mater 30(1):19–29

[31] Meng Y, Xia J, Zhu F, Zhang Y (2016) Synthesis of N-doped carbon by microwave-assisted pyrolysis ionic liquid for lithium-ion batteries. Int J Electrochem Sci 11:9881–9890

[32] Wang X, Dai S (2010) Ionic liquids as versatile precursors for functionalized porous carbon and carbon–oxide composite materials by confined carbonization. Angew Chem Int Ed 49(37):6664–6668

[33] Lee JS, Wang X, Luo H, Baker GA, Dai S (2009) Facile ionothermal synthesis of microporous and mesoporous carbons from task specific ionic liquids. J Am Chem Soc 131(13):4596–4597

[34] Zhi L, Hu YS, Hamaoui BE, Wang X, Lieberwirth I, Kolb U, Maier J, Müllen K (2008) Precursor-controlled formation of novel carbon/metal and carbon/metal oxide nanocomposites. Adv Mater 20(9):1727–1731

[35] Fulvio PF, Lee JS, Mayes RT, Wang X, Mahurin SM, Dai S (2011) Boron and nitrogen-rich carbons from ionic liquid precursors with tailorable surface properties. Phys Chem Chem Phys 13(30):13486–13491

[36] Lou YB, Liang J, Peng YL, Chen JX (2015) Ultra-small Co_3O_4 nanoparticles-reduced graphene oxide nanocomposite as superior anodes for lithium-ion batteries. Phys Chem Chem Phys 17(14):8885–8893

[37] Rahman MM, Wang J-Z, Deng X-L, Li Y, Liu H-K (2009) Hydrothermal synthesis of nanostructured Co_3O_4 materials under pulsed magnetic field and with an aging technique, and their electrochemical performance as anode for lithium-ion battery. Electrochim Acta 55(2):504–510

[38] Huang H, Gao S, Wu A-M, Cheng K, Li X-N, Gao X-X, Zhao J-J, Dong X-L, Cao G-Z (2017) Fe_3N constrained inside C nanocages as an anode for Li-ion batteries through post-synthesis nitridation. Nano Energy 31:74–83

[39] Zhang J, Zhang L, Yang S, Li D, Xie Z, Wang B, Xia Y, Quan F (2017) Facile strategy to produce N-doped carbon aerogels derived from seaweed for lithium-ion battery anode. J Alloy Compd 701:256–261

[40] Wang Q, Wu MY, Meng SJ, Zang XX, Dai ZY, Si WL, Huang W, Dong XC (2016) Hydrazine sensor based on Co_3O_4/rGO/carbon cloth electrochemical electrode. Adv Mater Interfaces 3(12). doi:10.1002/admi.201500691

[41] Wang B, Lu X-Y, Tang Y, Ben W (2016) General polyethyleneimine-mediated synthesis of ultrathin hexagonal Co_3O_4 nanosheets with reactive facets for lithium-ion batteries. ChemElectroChem 3(1):55–65

[42] Zhang G, Lu WT, Cao FF, Xiao ZD, Zheng XS (2016) N-doped graphene coupled with Co nanoparticles as an efficient electrocatalyst for oxygen reduction in alkaline media. J Power Sources 302:114–125

[43] Qu GL, Geng HB, Ge DH, Zheng JW, Gu HW (2016) Graphene-coated mesoporous Co_3O_4 fibers as an efficient anode material for Li-ion batteries. RSC Adv 6(75):71006–71011

[44] Li R, Wei Z, Gou X, Xu W (2013) Phosphorus-doped graphene nanosheets as efficient metal-free oxygen reduction electrocatalysts. RSC Adv 3(25):9978–9984

[45] Reddy ALM, Srivastava A, Gowda SR, Gullapalli H, Dubey M, Ajayan PM (2010) Synthesis of nitrogen-doped graphene films for lithium battery application. ACS Nano 4:6337–6342

[46] Li D, Shi D, Chen Z, Liu H, Jia D, Guo Z (2013) Enhanced rate performance of cobalt oxide/nitrogen doped graphene composite for lithium ion batteries. RSC Adv 3(15):5003–5008

[47] Li Y, Zhao Y, Cheng H, Hu Y, Shi G, Dai L, Qu L (2012) Nitrogen-doped graphene quantum dots with oxygen-rich functional groups. J Am Chem Soc 134(1):15–18

[48] Lin Z, Waller G, Liu Y, Liu M, Wong C-P (2012) Facile synthesis of nitrogen-doped graphene via pyrolysis of graphene oxide and urea, and its electrocatalytic activity toward the oxygen-reduction reaction. Adv Energy Mater 2(7):884–888

[49] Wang X, Li X, Zhang L, Yoon Y, Weber PK, Wang H, Guo J, Dai H (2009) N-doping of graphene through electrothermal reactions with ammonia. Science 324(5928):768–771

[50] Bulusheva LG, Okotrub AV, Kurenya AG, Zhang H, Zhang H, Chen X, Song H (2011) Electrochemical properties of nitrogen-doped carbon nanotube anode in Li-ion batteries. Carbon 49(12):4013–4023

[51] Wang R, Liu P, Lang J, Zhang L, Yan X (2017) Coupling effect between ultra-small Mn_3O_4 nanoparticles and porous carbon microrods for hybrid supercapacitors. Energy Storage Mater 6:53–60

[52] Guo L, Ding Y, Qin C, Li W, Du J, Fu Z, Song W, Wang F (2016) Nitrogen-doped porous carbon spheres anchored with Co_3O_4 nanoparticles as high-performance anode materials for lithium-ion batteries. Electrochim Acta 187:234–242

[53] Wu FF, Ma XJ, Feng JK, Qian YT, Xiong SL (2014) 3D Co_3O_4 and CoO@C wall arrays: morphology control, formation mechanism, and lithium-storage properties. J Mater Chem A 2(30):11597–11605

[54] Hu R, Zhang H, Bu Y, Zhang H, Zhao B, Yang C (2017) Porous Co_3O_4 nanofibers surface-modified by reduced graphene oxide as a durable, high-rate anode for lithium ion battery. Electrochim Acta 228:241–250

[55] Yin D, Huang G, Sun Q, Li Q, Wang X, Yuan D, Wang C, Wang L (2016) RGO/Co_3O_4 composites prepared using GO-MOFs as precursor for advanced lithium-ion batteries and supercapacitors electrodes. Electrochim Acta 215:410–419

[56] Cabana J, Monconduit L, Larcher D, Palacin MR (2010) Beyond intercalation-based Li-ion batteries: the state of the art and challenges of electrode materials reacting through conversion reactions. Adv Mater 22(35):E170–E192

[57] Xing X, Liu RL, Liu SQ, Xiao S, Xu Y, Wang C, Wu DQ (2016) Surfactant-assisted hydrothermal synthesis of cobalt oxide/nitrogen-doped graphene framework for enhanced anodic performance in lithium ion batteries. Electrochim Acta 194:310–316

[58] Chae B-M, Oh E-S, Lee Y-K (2015) Conversion mechanisms of cobalt oxide anode for Li-ion battery: in situ X-ray absorption fine structure studies. J Power Sources 274:748–754

[59] Luo L, Wu J, Xu J, Dravid VP (2014) Atomic resolution study of reversible conversion reaction in metal oxide electrodes for lithium-ion battery. ACS Nano 8(11):11560–11566

[60] Zhu WJ, Huang H, Gan YP, Tao XY, Xia Y, Zhang WK (2014) Mesoporous cobalt monoxide nanorods grown on reduced graphene oxide nanosheets with high lithium storage performance. Electrochim Acta 138:376–382

[61] Fang H, Zhang S, Liu W, Du Z, Wu X, Xing Y (2013) Hierarchical Co_3O_4@multiwalled carbon nanotube nanocable films with superior cyclability and high lithium storage capacity. Electrochim Acta 108:651–659

[62] Liang Y, Li Y, Wang H, Zhou J, Wang J, Regier T, Dai H (2011) Co_3O_4 nanocrystals on graphene as a synergistic catalyst for oxygen reduction reaction. Nat Mater 10(10):780–786

[63] Wang G, Shen X, Yao J, Park J (2009) Graphene nanosheets for enhanced lithium storage in lithium ion batteries. Carbon 47(8):2049–2053

[64] Laruelle S, Grugeon S, Poizot P, Dollé M, Dupont L, Tarascon JM (2002) On the origin of the extra electrochemical capacity displayed by MO/Li cells at low potential. J Electrochem Soc 149(5):A627–A634

[65] Peng C, Chen B, Qin Y, Yang S, Li C, Zuo Y, Liu S, Yang J (2012) Facile ultrasonic synthesis of CoO quantum dot/-graphene nanosheet composites with high lithium storage capacity. ACS Nano 6(2):1074–1081